View metadata, citation and similar papers at core.ac.uk
brought to you by CORE
provided by Repository@Nottingham

Amphiphilic Gemini Pyridinium-mediated incorporation of Zn(II)meso-tetrakis(4-carboxyphenyl)porphyrin into water-soluble gold nanoparticles for photodynamic therapy

María E. Alea-Reyes,[a,b] Jorge Soriano,[c] Inma Mora-Espí,[c] Mafalda Rodrigues,[a,b] David A. Russell,[d] Leonardo Barrios,[c] and Lluïsa Pérez-García*[a,b,1]

a. Departament de Farmacologia, Toxicologia i Química Terapèutica, Universitat de Barcelona, Avda. Joan XXIII 27-31, 08028 Barcelona, Spain.
E-mail: mlperez@ub.edu
b. Institut de Nanociència i Nanotecnologia UB (IN2UB), Universitat de Barcelona, Avda. Joan XXIII 27-31, 08028 Barcelona, Spain.
c. Departament de Biologia Cel·lular, Fisiologia i Immunologia. Universitat Autònoma de Barcelona, Spain.
d. School of Chemistry, University of East Anglia, Norwich Research Park, Norwich, Norfolk, NR4 7TJ, UK.

Total number of words: 5564

Total number of figures: 4

Total number of tables: 0

[1] Present address: School of Pharmacy, The University of Nottingham, University Park, Nottingham, NG7 2RD, UK

Abstract:

Zn-containing porphyrins are intensely investigated for their ability to form reactive oxygen species and thereby being potent photosensitizers for use in photodynamic therapy (PDT). Some of the drawbacks of the PDT approach, such as unspecific distribution, could be addressed by means of photosensitizer drug delivery systems. In this work, we synthesize and characterize new water-soluble gold nanoparticles (GNP) stabilized by a mixture of a polyethyleneglycol-containing thiol (to improve water solubility) and a new amphiphilic gemini-type pyridinium salt, which also acts as promotor of the incorporation of the anionic photosensitizer **Na-ZnTCPP** into the GNP. The obtained GNP have sizes between 7-10 nm, as observed by Transmission Electron Microscopy. The incorporation of the photosensitizer caused an increase in the hydrodynamic size, detected by Dynamic Light Scattering, as well as a shift in the Surface Plasmon Resonance peak on the GNP UV-visible absorption spectra. The presence of the photosensitizer in the GNP was corroborated using Fluorescence Spectroscopy. The amount of **Na-ZnTCPP** was found to be 327 molecules per GNP. The porphyrin-containing **Na-ZnTCPP-1·GNP** showed good enhanced ability to produce singlet oxygen, compared to free **Na-ZnTCPP**. Their cytotoxicity and phototoxicity were investigated *in vitro* using two different human breast cell lines, one of tumoral origin (SKBR-3) and another of normal epithelium origin (MCF-10A). SKBR-3 cells showed higher sensitivity to **Na-ZnTCCP** and **Na-ZnTCPP-1·GNP** in dark conditions. After irradiation, no significant differences were observed between both cell lines except for 1μM **Na-ZnTCCP-1·GNP** where SKBR-3 cells were also more sensitive.

Keywords: Gemini pyridinium amphiphiles, water-soluble gold nanoparticles, anionic porphyrin encapsulation, in vitro phototoxicity, photodynamic therapy, MCF-10A and SKBR-3 cell lines

Introduction

PDT is an approach of cancer treatment based on the use of specific drugs, called photosensitizers, which can induce cell death after irradiation, due to the formation of reactive oxygen species [1–3]. PDT has several advantages in the treatment of cancer, since it is less invasive, minimizes the secondary effects and allows more localized areas of the body to be treated. The major drawbacks of PDT are the non-specific distribution of the photosensitizer into the body, and the water-solubility of the photosensitizer, which can be low and thus requires a formulation to improve the administration. In particular, porphyrins are one of the most studied photosensitizers in the last years, to be applied in PDT [2,4–7] but also in sensors as hosts for molecular recognition [8,9]. One of the main characteristics of the porphyrin's structure is the possibility to incorporate a metal into its core, in particular bivalent cations such as Zn^{2+}, Mg^{2+}, Co^{2+} or Fe^{2+}. These metalloporphyrins are intensely investigated for their ability to form Reactive Oxygen Species (ROS) and thereby their interest as potent photosensitizers for use in PDT [6,10]. Furthermore, metalloporphyrins (especially Zn-containing porphyrin) have shown to be more efficient as photosensitizer in PDT than the metal-free porphyrin [11]. However, they frequently present low water solubility, which results in low distribution and consequently low efficiency. One way to overcome this drawback is by conjugating the molecule with a system that is used as vehicle.

In the last years, nanostructured systems have raised huge interest in the biomedical field because of their biocompatibility and the potential application as delivery agents for therapy [1,12,13]. One example is the use of such vehicles to target cells in cancer therapy [14]. One of the most studied systems in drug delivery is GNP [15,16], and the use of

nanoparticles incorporating photosensitizers to improve their specificity in PDT has been reported [5,6,17,18].

For the synthesis of organic and water soluble GNP, different types of ligands have been studied as stabilizers, like water-soluble polymers [19], amino acid based amphiphiles [20] or peptides [21]. The use of pyridinium salts as stabilizer agents of GNP has also been reported [22]. On the other hand, gemini surfactants display excellent properties in the preparation and stabilization of monodisperse GNP (organic and water soluble GNP) [13,23,24]. However, to the best of our knowledge, the synthesis and stabilization of GNP coated with pyridinium-based gemini amphiphiles and the incorporation of metalloporphyrins into such systems has not yet been reported. In this context, this study describes the methodology for the synthesis of pyridinium-coated GNP, based on a monophasic method, where the gemini-pyridinium amphiphile **1·2Br** acts as a promoter, a stabilizer agent as well as a host for the subsequent incorporation of the anionic photosensitizer **Na-ZnTCPP** into the **Na-ZnTCPP**, **1·GNP** (Figure 1). The new water-soluble GNP were characterized using UV-visible Absorption Spectroscopy, Transmission Electron Microscopy (TEM), Dynamic Light Scattering (DLS) and Fluorescence Spectroscopy. Furthermore, the production of singlet oxygen after irradiation was measured for the porphyrin **Na-ZnTCPP**, **1·GNP** (a control which does not contain photosensitizer) and **Na-ZnTCPP-1·GNP**, and the cytotoxicity as well as the phototoxicity of the **1·GNP** and **Na-ZnTCPP-1·GNP** were also analysed in two different Human Breast cell lines, one of tumoral origin (SKBR-3) and one of normal epithelium origin (MCF-10A).

Materials and methods

Materials: Ethanol (EtOH), methanol (MeOH), sodium borohydride ($NaBH_4$), gold (III) chloride trihydrate ($HAuCl_4 \cdot 3H_2O$) and 9,10-anthracenediyl-bis(methylene)dimalonic

acid (ABMA) were purchased from Sigma-Aldrich (Germany). α-thio-ω-carboxy-polyethylene glycol (HS-C_{11}-$(EG)_6$-COOH) was purchased from Prochimia (France).

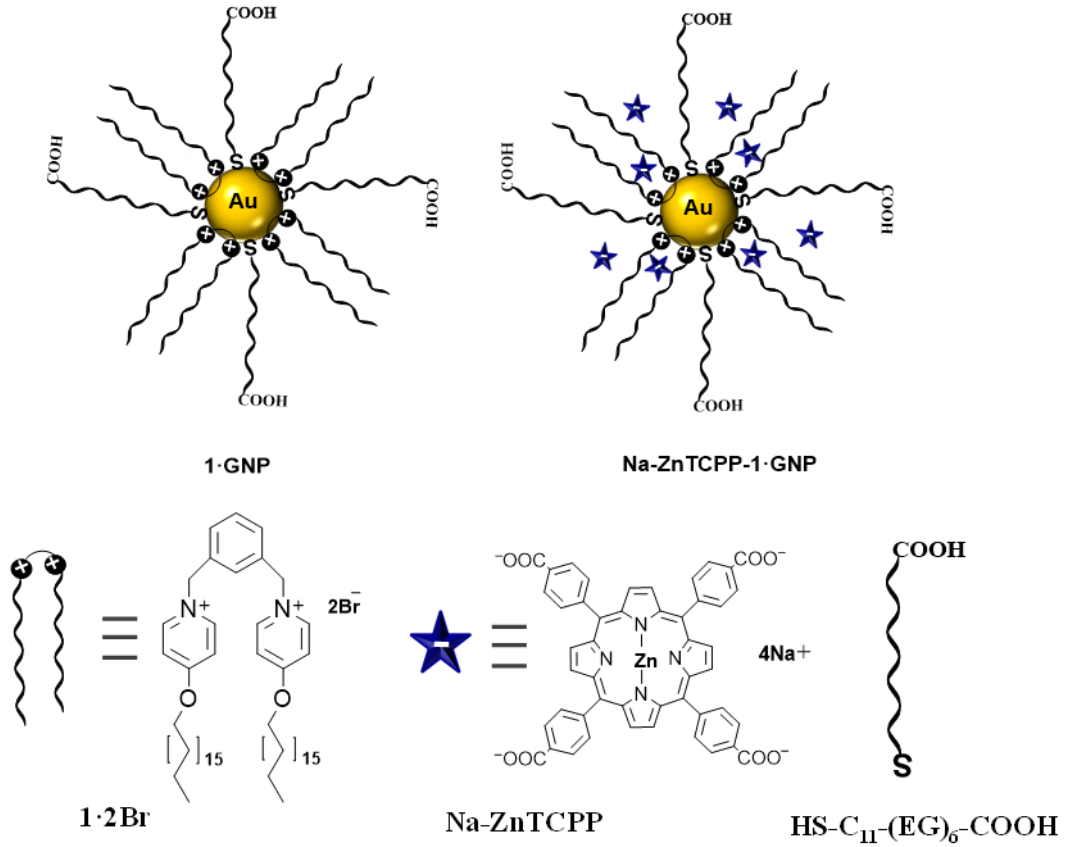

Figure 1. Schematic representation of **Na-ZnTCPP-1·GNP**.

Synthesis of compounds 1·2Br and Na-ZnTCPP

The synthesis and characterization of bis-pyridinium salt **1·2Br** follows a previously reported procedure for imidazolium analogues [23], ; in the case of the porphyrin **Na-ZnTCPP** they are explained in detail in the Supplementary Material (Section 1).

Synthesis of water-soluble gold nanoparticles 1·GNP and Na-ZnTCPP-1·GNP

A solution of α-thio-ω-carboxy-polyethylene glycol (1.3 mg, 0.0024 mmol) in water (1 mL) and a solution of bis-pyridinium salt **1·2Br** (5 mg, 0.0052 mmol) in EtOH (2 mL) were added to a stirred solution of $HAuCl_4 \cdot 3H_2O$ (6.7 mg, 0.017 mmol) in water (1 mL). $NaBH_4$ (3.3 mg, 0.087 mmol) in water (1mL) was added dropwise to the mixture at room temperature. The stirring continued for 24 h in the dark at room temperature. After this

time the solvent was removed in a rotary evaporator, and the red residue was purified by multiple cycles of washing with EtOH (3 x 1 mL) and water (3 x 1 mL) and centrifugation (14000 rpm, 17 min at 15 °C). The new water-soluble GNP were named **1·GNP**. For the incorporation of the porphyrin, a solution of **Na-ZnTCPP** (2 mg, 0.0021 mmol) in water (2 mL) was added to a stirred solution of 10 ml of **1·GNP** (3 x 10^{-3} μM) in water. The stirring continued for 24 h in the dark at room temperature. The solvent was removed in a rotary evaporator, followed by multiple cycles of washing with water (5 x 1 mL) and centrifugation (14000 rpm, 17 min at 15 °C), in order to eliminate the unbound porphyrin **Na-ZnTCPP**. These gold nanoparticles, named **Na-ZnTCPP-1·GNP**) were obtained at the concentration of 2.9 x 10^{-3} μM.

The GNP were characterized using the following techniques: UV-visible absorption spectra were recorded on a UV-1800 Shimadzu UV Spectrophotometer, using quartz cuvettes with a 1 cm path length. Fluorescence excitation and emission spectra were recorded on a Hitachi F-4500 Fluorescence Spectrometer, using quartz cuvettes with a 1 cm path length. TEM was performed at the *Centres Científics i Tecnològics de la Universitat de Barcelona* (CCiT-UB). The samples were prepared by drop casting a 2 x 10^{-3} μM aqueous solution of **1·GNP** or **Na-ZnTCPP-1·GNP** over a carbon-coated copper grid, and were observed using a Tecnai SPIRIT Microscope (FEI Co.) at 120 kV. The images were captured by a Megaview III camera and digitalized with the iTEM program. The size of the GNP core was measured with ImageJ. DLS analysis was carried out using a Zetasizer Nano ZS series (Malvern Instruments) from *Departament de Farmàcia, Tecnologia Farmacèutica i Fisicoquímica* at the *Universitat de Barcelona.*

Singlet Oxygen production of Na-ZnTCPP and Na-ZnTCPP-1·GNP

In a quartz cuvette, 3 μL of a solution of ABMA (0.2 mg, 0.51 mM) in MeOH (1 mL) was added to either **Na-ZnTCPP** (4.34 μL, 3 μM) or **Na-ZnTCPP-1·GNP** (485 μL, 3

μM of incorporated porphyrin) in water. The final volume (1.5 mL) in the cuvettes was completed with water and the solutions were thoroughly stirred. A light source in the range between 400 and 500 nm was used to irradiate the mixture during 4 h, using a laser power of 0.16 mw/cm^2. The laser was located 3 cm away from each cuvette. Fluorescence emission spectra were recorded every hour, in the range of 390-600 nm, and singlet oxygen production was determined by the decrease of the fluorescence intensity of ABMA at 431 nm.

Cell culture

All experiments were performed with two human mammary epithelial cell lines, one with non-tumorigenic origin (MCF-10A) and another tumorigenic (SKBR-3). Both cell lines were purchased from American Type Culture Collection (ATCC, Manassas, VA, USA). MCF-10A cells were cultured in DMEM/F12 (Gibco, Paisley, United Kingdom) supplemented with 5% horse serum (Gibco), 20 ng/ml epidermal growth factor (Gibco), 0.5 mg/ml hydrocortisone (Sigma-Aldrich), 100 ng/ml cholera toxin (Sigma-Aldrich) and 10 μg/ml insulin (Gibco). SKBR-3 cells were cultured in McCoy's 5A modified medium (Gibco) supplemented with 10% fetal bovine serum (Gibco). Both cell lines were maintained at 37°C and 5% CO_2 (standard conditions).

For each experiment, cells were seeded in 24-well dishes, with or without coverslips, at a density of 50,000 cells/well. Treatments were performed 24 h after seeding.

Photodynamic treatments

Cells were incubated in serum-free medium with different concentrations of **Na-ZnTCPP** (1 and 3 μM), **1·GNP** (70 and 200 μg/ml) or **Na-ZnTCPP-1·GNP** (1 and 3 μM, corresponding to 70 and 200 μg/ml of **1·GNP** respectively) for 24 h. Afterwards, cells were washed thrice with Phosphate-Buffered Saline (PBS) and maintained in culture medium during irradiation and post-treatment. Irradiation was performed for 10 min using

a PhotoActivation Universal Light device (PAUL, GenIUL, Barcelona, Spain), in the range of 620-630 nm (red light) and with a mean intensity of 55 mW/cm^2.

To evaluate the toxicity of **Na-ZnTCPP** and **Na-ZnTCPP-1·GNP** in absence of irradiation, cells were also incubated in the presence of both compounds as described above and were kept in dark conditions (Dark toxicity, DT).

In vitro cytotoxicity assay

Cell viability was evaluated 24 h after treatments by the 3-(4,5-dimethylthiazol-2-yl)-2,5diphenyltetrazolium bromide (MTT) assay (Sigma-Aldrich). The absorbance was recorded at 540 nm using a Victor 3 Multilabel Plate Reader (PerkinElmer, Waltham, MA, USA). For each treatment, viability was calculated as the absorbance of treated cells normalized to control conditions. Three independent experiments were performed in each case.

All graphics and statistical analyses were performed using GraphPad Prism version 6.01 for Windows, (GraphPad Software, La Jolla, California, USA). Results were analysed through a two-way ANOVA with a minimal significance level set at $P \leq 0.05$.

Actin microfilaments and nuclear staining

At 24 h after photodynamic treatments, cells were fixed with 4% paraformaldehyde in PBS for 15 min, permeabilized with 0,1% Triton X-100 (Sigma-Aldrich) in PBS and incubated with Alexa-Fluor®594-conjugated Phalloidin (Invitrogen) for 45 min. Next, cells were washed thrice and nuclei were counterstained with 5 µg/ml Hoechst 33258 (H-33258, Life Technologies, Carlsbad, CA) for 3 min. Preparations were mounted in ProLong Gold (Life Technologies) and observed under a Confocal Laser Scanning Microscope (CLSM, Olympus XT7) from the *Servei de Microscòpia* at the *Universitat Autònoma de Barcelona.*

Results and discussion

Synthesis and characterization of 1·2Br and Na-ZnTCPP

The bis-pyridinium salt **1·2Br** was selected to be used as stabilizer agent of GNP and also acts as host in the subsequent incorporation of the photosensitizer **Na-ZnTCPP**.

According to previous reports by our group [12,13,23], GNP stabilized with gemini imidazolium based amphiphiles showed good ability to incorporate anionic molecules. The gemini pyridinium analogue **1·2Br** is expected to expand the range of non-covalent interaction with anionic species. Consequently, the anionic porphyrin **Na-ZnTCPP** was selected in this work to be incorporated on the synthesized pyridinium-based GNP. **Na-ZnTCPP** was synthesized according to modification of previously reported methods [25,26]. The metalation step was monitored by UV-visible Absorption Spectroscopy: the four Q bands from the free base porphyrin are replaced by two Q bands of the corresponding Zn(II) derivative, indicating the metalation process is complete in 24 h. **Na-ZnTCPP** was obtained with a 94% yield (synthesis and characterization are explained in detail in Supplementary Material Section 1, Scheme S1 and Figures S1-S4).

Synthesis of water-soluble gold nanoparticles 1·GNP and Na-ZnTCPP-1·GNP

In order to obtain nanoparticles with a high potential use in biomedical applications, the synthesized GNP should be water soluble. For this reason, we used a mixture of the gemini pyridinium-based amphiphilic ligand **1·2Br** and the thiolated polyethyleneglycol derivative α-thio-ω-carboxy-polyethylene glycol for the formation of all the new GNP. Briefly, the GNP were synthesized by preparing small amounts of α-thio-ω-carboxy-polyethylene glycol in EtOH, to favour the solubility in water of synthesized GNP, and **1·2Br** as stabilizer agent and anionic binder; then adding an aqueous solution of $HAuCl_4$ and then the reducing agent $NaBH_4$. The obtained GNP were purified by sequential

washing and centrifugation, and were named **1·GNP**. These new water-soluble **1·GNP** were later used as a model colloid for the biological control experiments.

In this work, we selected the anionic porphyrin **Na-ZnTCPP** as photosensitizer to be incorporate into the gemini-pyridinium coated GNP. This porphyrin has already shown high potential for use in PDT [27,28] due to its water solubility, and its negative charges allows its noncovalent incorporation into cationic GNP, thus providing an alternative delivery strategy with the potential to avoid photosensitizer leakage and processing issues, which has been reported for different drugs [29,30]. The anionic porphyrin **Na-ZnTCPP** was incorporated on **1·GNP**, and the **Na-ZnTCPP** containing GNP were named **Na-ZnTCPP-1·GNP**. The schematic representation of **1·GNP** and **Na-ZnTCPP-1·GNP** can be seen in Figure 1.

Characterization of Na-ZnTCPP, 1·GNP and Na-ZnTCPP-1·GNP

The formation of **1·GNP** and the incorporation of the porphyrin **Na-ZnTCPP** into the **Na-ZnTCPP-1·GNP** were confirmed by UV-visible Absorption Spectroscopy (Figure 2 a)). The UV-visible absorption spectra were recorded in water. The free porphyrin **Na-ZnTCPP** showed the typical Soret band at 423 nm and two Q bands at 557 and 593 nm. In the case of **1·GNP**, the typical Surface Plasmon Resonance (SPR) band of the GNP was observed near 520 nm, while the **Na-ZnTCPP-1·GNP** show a peak at 530 nm, and also a peak at *ca.* 430 nm that corresponds to the porphyrin **Na-ZnTCPP** Soret band. In addition, the two typical Zinc porphyrin Q bands can be identified in the **Na-ZnTCPP-1·GNP** spectrum, at 566 and 610 nm. It is noteworthy the observation of shifts in the peaks when comparing: a) the Soret band wavelength of the free porphyrin **Na-ZnTCPP** (423 nm) with the porphyrin incorporated into **Na-ZnTCPP-1·GNP** (430 nm), b) the typical SPR band of **1·GNP** (520 nm) and of **Na-ZnTCPP-1·GNP (**530 nm) and c) the Q bands of the free porphyrin (557 and 593) and the porphyrin incorporated in the **Na-**

ZnTCPP-1·GNP (566 and 610 nm). These shifts in the characteristic peaks are probably due to the influence of the electrostatic interaction established between the positive charges of the pyridinium salt **1·2Br** and the negative charges of the porphyrin **Na-ZnTCPP** present in the **Na-ZnTCPP-1·GNP**, where the alkyl chains may create a pocket where the porphyrin is introduced in the proximity of the polar head, but also the porphyrin may be localized outside the pocket but interacting with the positive charge of the **1·2Br**.

1·GNP and **Na-ZnTCPP-1·GNP** were characterized using TEM to study their morphology and their size distribution for **1·GNP** and **Na-ZnTCPP-1·GNP** as seen in Figure 2 (see Supplementary Material Section 2 Figure S5). The analysed GNP display a spherical shape and show sizes between 7-10 nm. In both cases, the particles are well separated and in very few cases show short distances between them, indicating they are well dispersed in water and that the incorporation of **Na-ZnTCPP** did not cause aggregation.

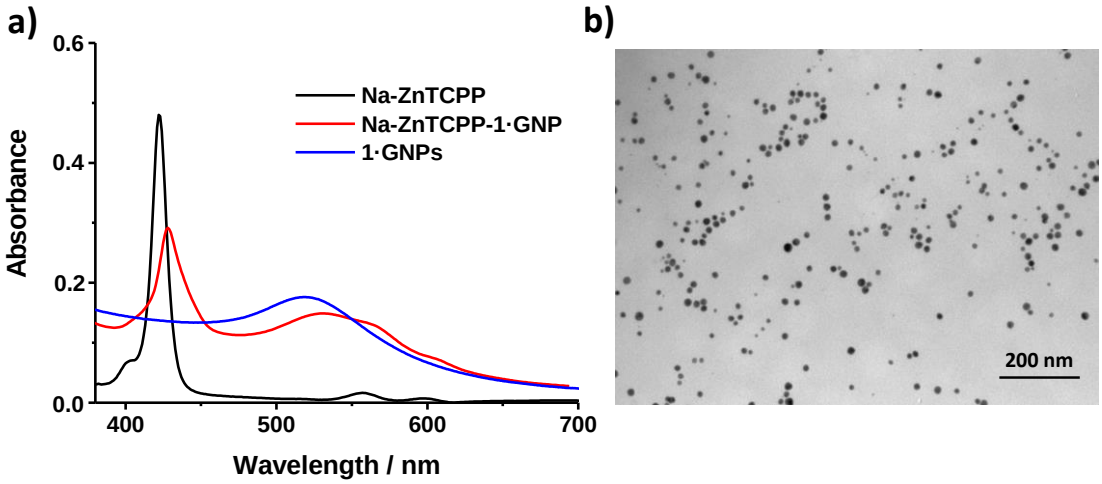

Figure 2. a) UV-visible absorption spectra of the free porphyrin **Na-ZnTCPP**, **1·GNP** and **Na-ZnTCPP-1·GNP**, recorded in water at 25 °C and b) Transmission electronic microscopy (TEM) image of **Na-ZnTCPP-1·GNP**.

1·GNP and **Na-ZnTCPP-1·GNP** were also analysed using DLS. Both GNP proved stable in solution, since no aggregation occurred, and have a low polydispersity index, with values of 0.13 and 0.21, respectively. The average size measured was of 10.2 nm for **1·GNP** and 15.3 nm for **Na-ZnTCPP-1·GNP**. DLS measured the hydrodynamic diameter that includes not only the core but also the alkyl chains of the **1·2Br**, the thiol α-thio-ω-carboxy-polyethylene glycol and the molecules of the incorporated porphyrin **Na-ZnTCPP**. The sizes obtained by DLS for **1·GNP** and **Na-ZnTCPP-1·GNP** are different, which may be due to the incorporation of the porphyrin in the organic layer around the gold core that leads to an increase in the diameter of the nanoparticles **Na-ZnTCPP-1·GNP** in relation with **1·GNP**.

Fluorescence spectroscopy was also used to identify the incorporation of the porphyrin into the synthesized **Na-ZnTCPP-1·GNP**. Fluorescence emission spectra were recorded in water for the free porphyrin **Na-ZnTCPP** and **Na-ZnTCPP-1·GNP** (see Supplementary Material Section 2 Figure S6), and both spectra exhibit two peaks at *ca.* λ 606 nm and λ 660 nm following excitation at λ 421 nm, which is consistent with reports for Zn-porphyrin derivatives [31]. These results confirm the incorporation of **Na-ZnTCPP** into the **Na-ZnTCPP-1·GNP**, and also demonstrate that the fluorescence emission of the photosensitizer is not affected significantly when the porphyrin is linked to the GNP.

Quantification of Na-ZnTCPP incorporated into Na-ZnTCPP-1·GNP

The quantification of the amount of porphyrin **Na-ZnTCPP** per **Na-ZnTCPP-1·GNP** was performed using UV-vis absorption spectroscopy and taking into account the diameter size of **Na-ZnTCPP-1·GNP**, as previously determined by TEM. The wavelength selected to determine the amount of **Na-ZNTCPP** incorporated into **Na-ZnTCPP-1·GNP** was that corresponding to the Soret band (430 nm) because it was the

most intense peak corresponding to the porphyrin. First, a calibration curve of **Na-ZnTCPP** was obtained using a range of concentrations between 0.5 µM and 10 µM (see Supplementary Material Section 3 Figure S7), in order to calculate its extinction coefficient (ε), that was found to be (ε_{423}) = 355600 M^{-1} cm^{-1}. The **Na-ZnTCPP-1·GNP** UV-Visible absorption spectrum shows quite broad absorption bands and in order to normalize the Soret band absorbance value, a subtraction between the Soret band peak and the absorbance of the porphyrin into **Na-ZnTCPP-1·GNP** sloping background at 470 nm was calculated (see Supplementary Material Section 3 Figure S8). Accordingly, we calculated that the molarity of the **Na-ZnTCPP** present on the **Na-ZnTCPP-1·GNP** colloidal suspension corresponds to 0.94 µM. Consequently, in order to obtain the number of porphyrin molecules per **Na-ZnTCPP-1·GNP**, the concentration of the **Na-ZnTCPP-1·GNP** colloidal suspension was calculated using the diameter obtained by TEM and its UV absorbance value at 450 nm, obtaining a value of 2.9 x 10^{-3}µM. Taking into account the suspension volume (3 mL) and the Avogadro's number, we obtain the number of porphyrin molecules immobilized on the **Na-ZnTCPP-1·GNP** surface, which corresponds to 327 molecules of **Na-ZnTCPP** incorporated per GNP (see Supplementary Material Section 3 Table S1).

Singlet oxygen production of Na-ZnTCPP and Na-ZnTCPP-1·GNP

Singlet oxygen ($^1O_2$) production was examined using water soluble ABMA as a probe. Upon reaction with $^1O_2$, ABMA forms a non-fluorescent 9,10-endoperoxide product [32], resulting in the decay of the fluorescence of ABMA, which can be easily monitored using fluorescence spectroscopy. The photosensitizer **Na-ZnTCPP**, both free in aqueous solution or incorporated into **Na-ZnTCPP-1·GNP** in water, was irradiated for 4 h with continuous stirring in the presence of a solution of ABMA in MeOH, using a blue light source which excites the Soret band of the porphyrin (near 420 nm). The fluorescence

emission spectra were recorded every hour, in the range of 390-600 nm, and the singlet oxygen production was determined by the decrease of the fluorescence intensity of ABMA (see Supplementary Material Section 4 Figure S9). A similar protocol was followed to quantify the $^1O_2$ production by **1·GNP** as control. The percentage decay of ABMA fluorescence emission band at λ 431 nm following irradiation of **Na-ZnTCPP**, **Na-ZnTCPP-1·GNP** and **1·GNP** is shown in Supplementary Material Section 4 Figure S10. It can be clearly observed the fluorescence decay in the case of **Na-ZnTCPP** and **Na-ZnTCPP-1·GNP**, demonstrating the formation of singlet oxygen. However, when ABMA solution was irradiated under the same conditions in the presence of **1·GNP**, without any porphyrin, a negligible decay in the ABMA fluorescence was observed, confirming that the singlet oxygen was produced by the photosensitizer **Na-ZnTCPP**, alone or incorporated in the GNP, upon irradiation. After 4 hours, the percentage of emission decay for ABMA in the presence of **Na-ZnTCPP** and **Na-ZnTCPP-1·GNP** was 30% and 49%, respectively, indicating that the porphyrin incorporated into **Na-ZnTCPP-1·GNP** is more efficient to produce the $^1O_2$ than the free porphyrin in solution. To further compare the ability to produce singlet oxygen by **Na-ZnTCPP** both free in solution and incorporated in the **Na-ZnTCPP-1·GNP**, the maximum rate of ABMA photobleaching was normalized with the concentration of the photosensitizer **Na-ZnTCPP** (3 μM) (see Supplementary Material Section 4 Equation S1). The calculated maximum rates of ABMA photobleaching upon irradiation were 0.03% *IF*/min·μM obtained for the free porphyrin **Na-ZnTCPP**, and 0.08% *IF*/min·μM obtained for the porphyrin-containing **Na-ZnTCPP-1·GNP**, where *IF* is the Intensity of Fluorescence (see Supplementary Material Section 4 Figure S11). These results demonstrate that the porphyrin **Na-ZnTCPP** resulted more effective when immobilized on GNP rather than free in solution, with an increased singlet oxygen production, a feature previously

reported for similar systems [2,33]. This fact is even more remarkable considering that the photobleaching of the porphyrin incorporated into GNP was measured in aqueous solution, where oxygen is much less soluble and usually leads to a less significant effect for this type of measurement because of the shorter lifetime of singlet oxygen in water [34].

Although there are examples in the literature reporting similar strategies to probe the singlet oxygen production, a direct comparison is difficult, because different conditions are used: for example, different photosensitizers (phtalocyanines [33], porphyrin [2,35] and metalloporphyrins [36]), light sources, irradiation times, different vehicles and different anthracene derivatives, such as ABMA, DMA (9,10-dimethyl-anthracene) and ADPA (9-[(2,2′-dipicolylamino)methyl]anthracene)[32,35,37], used to detect reactive oxygen species in particular singlet oxygen.

Photodynamic effect of Na-ZnTCPP on cell cultures

Cell viability 24 h after treatments with **Na-ZnTCPP** was evaluated by MTT assay (see Supplementary Material Section 5 Figure S12). In dark conditions, incubation with 1 µM **Na-ZnTCPP** did not significantly modify the viability of MCF-10A cells, whereas treatments with a higher concentration (3 µM **Na-ZnTCPP**) induced a decrease in cell survival. In contrast, SKBR-3 cells showed a decrease in cell viability at both concentrations. When irradiated (10 min), both cell lines, treated either with 1 and 3 µM **Na-ZnTCPP**, showed a significant decrease in cell survival, but without significant differences between both cell lines, in accordance to preliminary data [38].

Actin microfilaments and nuclear morphology were observed by Alexa-Fluor®594-conjugated Phalloidin and H-33258 staining. In absence of irradiation, both cell lines treated either with 1 or 3 µM **Na-ZnTCPP** did not present actin microfilaments or nuclear alterations (Figure 3 a) and c)). In contrast, after 10 min of irradiation, and at both

concentrations of **Na-ZnTCPP**, MCF-10A cells showed a high disorganization of actin microfilaments and no stress fibres were observed, although nuclei remained unaltered (Figure 3 b)). SKBR-3 cells after irradiation showed a similar disorganization of the actin cytoskeleton but some apoptotic or necrotic nuclei were observed (Figure 3 d)).

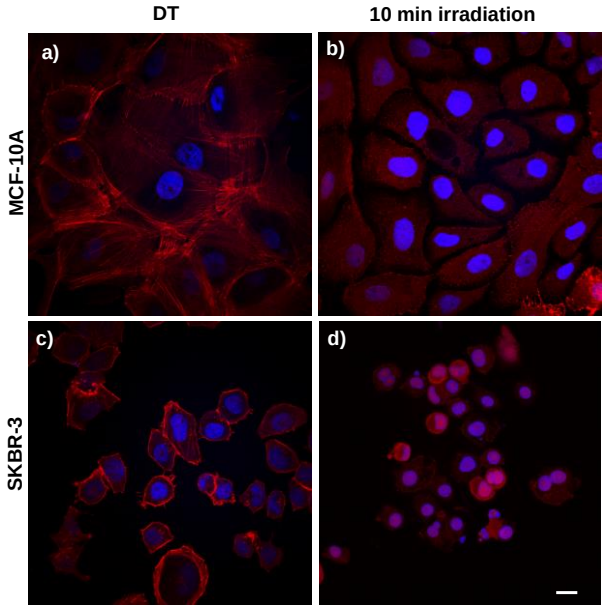

Figure 3. Cells incubated with 3µM **Na-ZnTCPP** for 24 h, kept in darkness (DT) and processed 24 h after with Alexa-Fluor®594-conjugated Phalloidin (red) and counterstained with Hoechst-33258 (blue) a) and c). Cells incubated with 3µM **Na-ZnTCPP** for 24 h, irradiated 10 min and processed 24 h after photodynamic treatments with Alexa-Fluor®594-conjugated Phalloidin (red) and counterstained with Hoechst-33258 (blue) b) and d). Scale bar, 10 µm.

Photodynamic effect of Na-ZnTCPP-1·GNP on cell cultures

Prior to the phototoxicity study of **Na-ZnTCPP-1·GNP**, the uptake and cytotoxicity of **1·GNP** in MCF-10A and SKBR-3 cells was evaluated. **1·GNP** uptake after 24 h incubation was observed under bright field microscope (see Supplementary Material

Section 5 Figure S13 a) and b)). In MCF-10A cells, the majority of nanoparticles were distributed around the nuclei forming aggregates of variable size. In contrast, SKBR-3 cells were able to internalize **1·GNP** but in a lesser quantity, and many remained attached to the plasma membrane. The effect of **1·GNP** on cell viability showed that 24 h after irradiation, the presence of **1·GNP** did not reduce significantly the viability of MCF-10A cells, but significantly reduced SKBR-3 cells survival at both studied concentrations (70 or 200 μg/ml), (see Supplementary Material Section 5 Figure S13 c)). Finally, the presence of **1·GNP** inside the cells did not alter actin cytoskeleton or nuclear morphology (see Supplementary Material Section 5 Figure S13 d)-g), and under bright field microscope we confirmed that **1·GNP** remained inside the cells, with a similar pattern to that previously described.

The cytotoxicity of **Na-ZnTCPP-1·GNP** 24 h after treatments was evaluated by MTT assay (see Supplementary Material Section 5 Figure S14). In dark conditions MCF-10A cells viability was not affected at both **Na-ZnTCPP-1·GNP** concentration. However, SKBR-3 cells showed a concentration-dependent decrease of cell survival. After irradiation, both cell lines showed a decrease in cell viability although MCF-10A treated with 1μM **Na-ZnTCPP-1·GNP** presented higher resistance to photodynamic treatments than MCF-10A cells treated with 3μM **Na-ZnTCPP-1·GNP** or SKBR-3 cells subjected to treatments with both concentrations of **Na-ZnTCPP-1·GNP**.

As observed for **1·GNP**, MCF-10A showed a higher uptake of **Na-ZnTCPP-1·GNP** than SKBR-3 cells (Figure 4 a) and c)). It has been reported that MCF-10A cells can internalize both positively and negatively charged particles, whereas in SKBR-3 cells the uptake of negative charged particles is low [39,40]. The differences in cell uptake can be explained because **Na-ZnTCPP-1·GNP** are negatively charged. After irradiation, most of MCF-10A cells treated with 1μM **Na-ZnTCPP-1·GNP** remained unaltered, but some detached

and contracted cells were observed (Figure 4 b)). On the contrary, most of the SKBR-3 cells subjected to the same treatments were floating in the medium and showed blebs in their plasma membrane (Figure 4 d)).

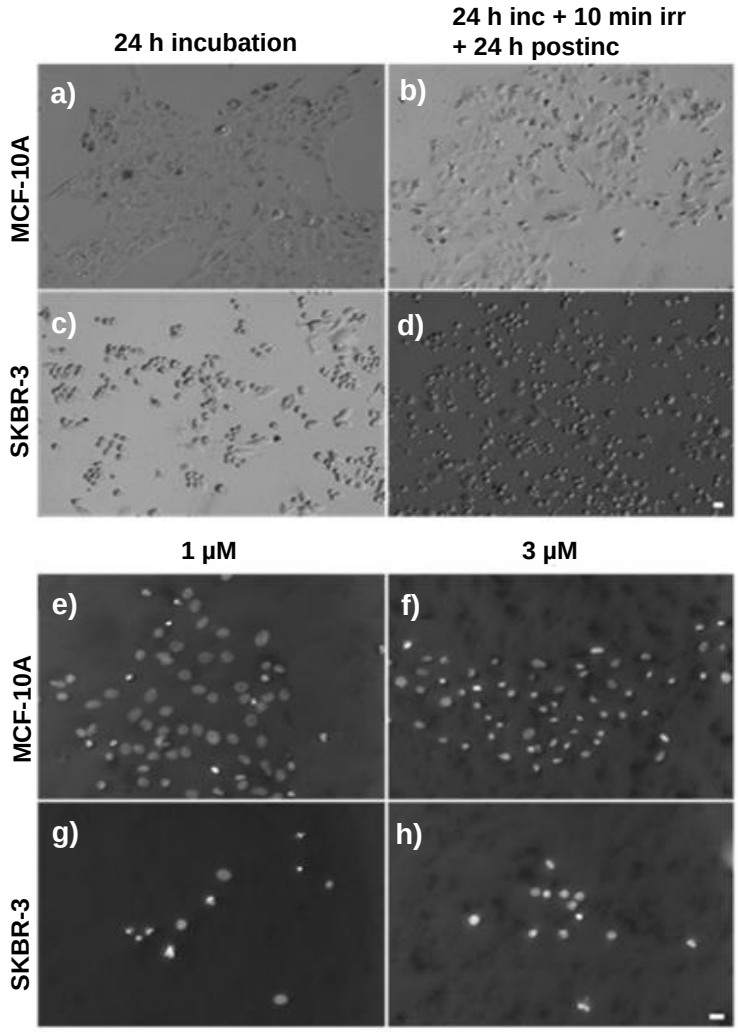

Figure 4. Cells incubated with 1µM **Na-ZnTCPP-1·GNP** for 24 h and observed under DIC microscope a) and c). Cells incubated with 1µM **Na-ZnTCPP-1·GNP** for 24 h, irradiated 10 min with red light and observed after 24 h under DIC microscope b) and d). Cells incubated with different concentrations of **Na-ZnTCPP-1·GNP** for 24 h, irradiated 10 min with red light and processed after 24 h for Hoechst-33258 staining e)-h). Scale bar, 10 µm.

Nuclear staining with H-33258 confirms these results: MCF-10A cells treated 1µM **Na-ZnTCPP-1·GNP** showed most of the nuclei unaltered, but with some apoptotic or necrotic nuclei (Figure 4 e)). In contrast, the same cells treated with 3µM **Na-ZnTCPP-1·GNP** showed a predominant necrotic morphology (Figure 4 f)). SKBR-3 cells treated with both concentrations of **Na-ZnTCPP-1·GNP** showed an important decrease in cell density and the cells that remained attached showed necrotic or apoptotic morphology (Figure 4 g) and h)).

Conclusion

In this work, we successfully prepared new water–soluble **1·GNP** based on bis-pyridinium amphiphiles **1·2Br** following a monophasic method using as stabilizer agents α-thio-ω-carboxy-polyethylene glycol, to make the nanoparticles water soluble, and the pyridinium salt **1·2Br**, which also acted as host to incorporate **Na-ZnTCPP** in the **Na-ZnTCPP-1·GNP**. The obtained porphyrin-loaded GNP are spherical and monodisperse, and the incorporation of the photosensitizer did not cause aggregation, thus suggesting they can be used as essentially single particle delivery system. The incorporation of the **Na-ZnTCPP** into the **Na-ZnTCPP-1·GNP** notably increased the capacity of the photosensitizer to generate singlet oxygen, which may be due to an enhancement effect of the GNP gold core on the porphyrin activity. SKBR-3 tumoral cells showed more sensitivity to **Na-ZnTCPP-1·GNP,** in dark conditions or after irradiation, than MCF-10A non-tumoral cells.

These findings suggest that the synthesized **Na-ZnTCPP-1·GNP** are a promising nanosystem for PDT. Future work includes the incorporation of antibodies through immobilization using the α-thio-ω-carboxy-polyethylene glycol present on the **Na-ZnTCPP-1·GNP**, to actively target cancer cells.

Appendix A. Supplementary data

Supplementary data related to this article can be found at http://dx.doi.org/10.1016/j.colsurfb.xxxx.xx.xxx.

Acknowledgements

This work was supported by the EU ERDF (FEDER) funds and the Spanish Government [grants TEC2014-51940-C2-2-R], [MAT2014-57960-C03-3-R] and the *Generalitat de Catalunya* [2014-SGR-524]. M. E. A-R and I. M-E thank the *Universitat de Barcelona* and the Spanish *Ministerio de Economía, Industria y Competitividad*, respectively, for predoctoral grants. The authors wish to thank the *Servei de Microscòpia* at the *Universitat Autonòma de Barcelona.*

References

[1] M. Triesscheijn, P. Baas, J.H.M. Schellens, F.A. Stewart, Oncol., 11 (2006) 1034–1044.

[2] O. Penon, M.J. Marín, D.A. Russell, L. Pérez-García, J. Colloid Interface Sci., 496 (2017) 100–110.

[3] H.-I. Lee, Y.-J. Kim, Colloids Surfaces B: Biointerfaces, 142 (2016) 182–191.

[4] E.D. Sternberg, D. Dolphin, C. Brückner, C. Brickner, Tetrahedron, 54 (1998) 4151–4202.

[5] O. Penon, T. Patiño, L. Barrios, C. Nogués, D.B. Amabilino, K. Wurst, L. Pérez-García, ChemistryOpen, 4 (2015) 127–136.

[6] P.M. Antoni, A. Naik, I. Albert, R. Rubbiani, S. Gupta, P. Ruiz-Sanchez, P. Munikorn, J.M.J.M. Mateos, V. Luginbuehl, P. Thamyongkit, U. Ziegler, G. Gasser, G. Jeschke, B. Spingler, Chem. - A Eur. J., 21 (2015) 1179–1183.

[7] Z. Hu, Y. Pan, J. Wang, J. Chen, J. Li, L. Ren, Biomed. Pharmacother., 63 (2009) 155–164.

[8] R. Yang, K. Li, K. Wang, F. Zhao, N. Li, F. Liu, Anal. Chem., 75 (2003) 612–621.

[9] H. Ogoshi, T. Mizutani, Curr. Opin. Chem. Biol., 3 (1999) 736–739.

[10] L. Jayashankar, B.S. Sundar, R. Vijayaraghavan, K.S. Betanabhatla, C. Ajm, J. Athimoolam, K.S. Saravanan, Pharmacologyonline, 1 (2008) 66–77.

[11] Q. Yu, W.-X. Xu, Y.-H. Yao, Z.-Q. Zhang, S. Sun, J. Li, J. Porphyrins Phthalocyanines, 19 (2015) 1107–1113.

[12] E. Amirthalingam, M. Rodrigues, L. Casal-Dujat, A.C. Calpena, D.B. Amabilino, D. Ramos-López, L. Pérez-García, J. Colloid Interface Sci., 437 (2015) 132–139.

[13] M. Rodrigues, A.C. Calpena, D.B. Amabilino, D. Ramos-López, J. de Lapuente, L. Pérez-García, RSC Adv., 4 (2014) 9279–9287.

[14] T. Stuchinskaya, M. Moreno, M.J. Cook, D.R. Edwards, D.A. Russell, Photochem. Photobiol. Sci., 10 (2011) 822–831.

[15] H. Bessar, I. Venditti, L. Benassi, C. Vaschieri, P. Azzoni, G. Pellacani, C. Magnoni, E. Botti, V. Casagrande, M. Federici, A. Costanzo, L. Fontana, G. Testa, F.F. Mostafa, S.A. Ibrahim, M.V. Russo, I. Fratoddi, Colloids Surfaces B: Biointerfaces, 141 (2016) 141–147.

[16] M. Ganeshkumar, M. Sathishkumar, T. Ponrasu, M.G. Dinesh, L. Suguna, Colloids Surfaces B: Biointerfaces, 106 (2013) 208–216.

[17] G.V. Roblero-Bartolon, E. Ramon-Gallegos, Gac. Med. Mex., 151 (2015) 85–98.

[18] K. Zaruba, J. Kralova, P. Rezanka, P. Pouckova, L. Veverkova, V. Kral, Org. Biomol. Chem., 8 (2010) 3202–3206.

[19] I. Hussain, S. Graham, Z. Wang, B. Tan, D.C. Sherrington, S.P. Rannard, A.I. Cooper, M. Brust, J. Am. Chem. Soc., 127 (2005) 16398–16399.

[20] S. Si, E. Dinda, T.K. Mandal, Chem. Eur. J., 13 (2007) 9850–9861.

[21] R. Lévy, N.T.K. Thanh, R.C. Doty, I. Hussain, R.J. Nichols, D.J. Schiffrin, M. Brust, D.G. Fernig, J. Am. Chem. Soc., 126 (2004) 10076–10084.

[22] K.B. Male, J.J. Li, C.C. Bun, S.C. Ng, J.H.T. Luong, J. Phys. Chem. C., 112 (2008) 443–451.

[23] L. Casal-Dujat, M. Rodrigues, A. Yagüe, A.C. Calpena, D.B. Amabilino, J. González-Linares, M. Borràs, L. Pérez-García, Langmuir, 28 (2012) 2368–2381.

[24] M. Murawska, A. Skrzypczak, M. Kozak, Acta Phys. Pol. A., 121 (2012) 888–892.

[25] M. Mojiri-Foroushani, H. Dehghani, N. Salehi-Vanani, Electrochim. Acta., 92 (2013) 315–322.

[26] Y. Yuan, H. Lu, Z. Ji, J. Zhong, M. Ding, D. Chen, Y. Li, W. Tu, D. Cao, Z. Yu, Z. Zou, Chem. Eng. J., 275 (2015) 8–16.

[27] N. Siraj, P.E. Kolic, B.P. Regmi, I.M. Warner, Chem. Eur. J., 21 (2015) 14440–14446.

[28] P.E. Kolic, N. Siraj, S. Hamdan, B.P. Regmi, I.M. Warner, J. Phys. Chem. C., 120 (2016) 5155–5163.

[29] C.K. Kim, P. Ghosh, C. Pagliuca, Z.J. Zhu, S. Menichetti, V.M. Rotello, J. Am. Chem. Soc., 131 (2009) 1360–1361.

[30] P. Basilion, C. Burda, J Am Chem Soc., 133 (2012) 2583–2591.

[31] V. V. Apanasovich, E.G. Novikov, N.N. Yatskov, R.B.M. Koehorst, T.J. Schaafsma, A. van Hoek, J. Appl. Spectrosc., 66 (1999) 613–616.

[32] M. Wang, L. Huang, S.K. Sharma, S. Jeon, S. Thota, F.F. Sperandio, S. Nayka, J. Chang, M.R. Hamblin, L.Y. Chiang, J. Med. Chem., 55 (2012) 4274–4285.

[33] R. Lin, L. Zhou, Y. Lin, A. Wang, J.H. Zhou, S.H. Wei, Spectroscopy, 26 (2011) 179–185.

[34] R. Battino, T.R. Rettich, T. Tominaga, J. Phys. Chem. Ref. Data., 12 (1983) 163–178.

[35] S.J. Mora, M.E. Milanesio, E.N. Durantini, J. Photochem. Photobiol. A Chem., 270 (2013) 75–84.

[36] O. Penon, M.J. Marín, D.A. Russell, L. Pérez-García, J. Colloid Interface Sci., 462 (2016) 154–165.

[37] S. Senthilkumar, R. Hariharan, A. Suganthi, M. Ashokkumar, M. Rajarajan, K. Pitchumani, Powder Technology, 237 (2013) 497-505.

[38] J. Soriano, I. Mora-Espí, M. E. Alea-Reyes, L. Pérez-García, L. Barrios, E. Ibáñez, C. Nogués, Sci. Rep., 7 (2017) 41340.

[39] T. Patiño, J. Soriano, E. Amirthalingam, S. Durán, A. González-Campo, M. Duch, E. Ibáñez, L. Barrios, J.A. Plaza, L. Pérez-García, C. Nogués, Nanoscale, 8 (2016) 8773–8783.

[40] T. Patiño, J. Soriano, L. Barrios, E. Ibáñez, C. Nogués, Sci. Rep., 5 (2015) 11371.